Research Square

Preprints are preliminary reports that have not undergone peer review.
They should not be considered conclusive, used to inform clinical practice,
or referenced by the media as validated information.

Photoswitching in P-Centered Bi- and Tetraradicaloid–Group 14 Metallocene Hybrids

Axel Schulz

axs001@hotmail.de

University of Rostock https://orcid.org/0000-0001-9060-7065

Zahra Tayebi

Leibniz Institut for catalysis https://orcid.org/0009-0007-8122-643X

Ritika Ritika

University of Rostock https://orcid.org/0009-0000-0083-4644

Karsten Lüdtke

University of Rostock https://orcid.org/0000-0003-0865-3500

Jonas Bresien

University of Rostock https://orcid.org/0000-0001-9450-3407

Fabian Reiß

Leibniz Institute for Catalysis

Olga Bokareva

Leibniz Institute for Catalysis https://orcid.org/0000-0002-2313-7996

Torsten Beweries

Universität Rostock

Article

Keywords:

Posted Date: April 21st, 2026

DOI: https://doi.org/10.21203/rs.3.rs-9390588/v1

License: This work is licensed under a Creative Commons Attribution 4.0 International License.
Read Full License

Additional Declarations: There is **NO** Competing Interest.

Photoswitching in P-Centered Bi- and Tetraradicaloid–Group 14 Metallocene Hybrids

Zahra Tayebi,[a,b] Ritika Ritika,[a,b] Karsten Paul Lüdtke,[a] Jonas Bresien,[a] Fabian Reiß,[b] Olga S. Bokareva,[b,c]* Torsten Beweries,[b]* and Axel Schulz[a,b]*

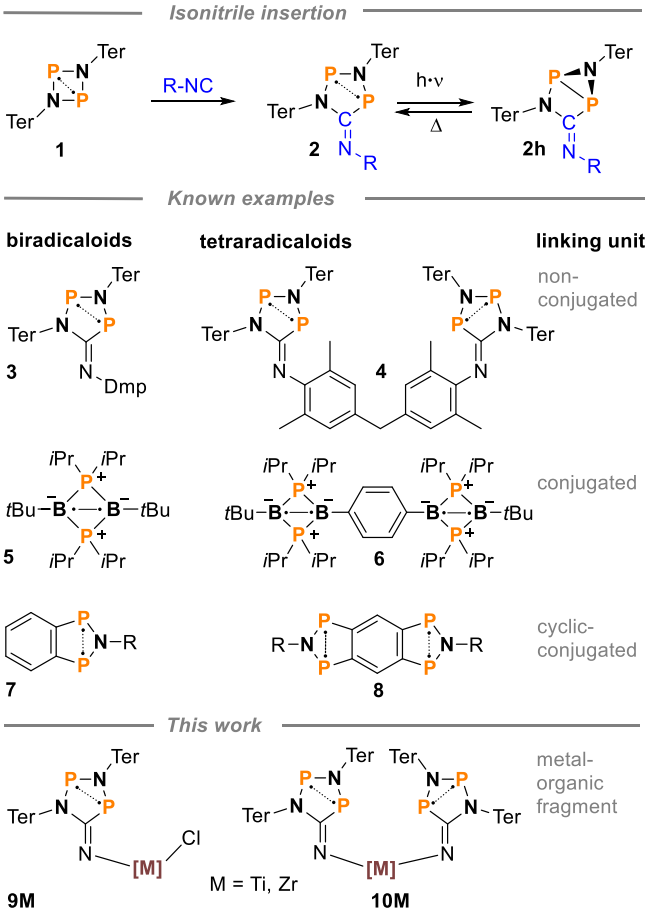
[a] Z. Tayebi , K. P. Lüdtke, Dr. J. Bresien, Prof. Dr. A. Schulz
[a]Institut für Chemie, Universität Rostock, Albert-Einstein-Straße 3a, D-18059 Rostock, Germany
E-Mail: axel.schulz@uni-rostock.de
[b] Z. Tayebi, R. Ritika, Dr. O. S. Bokareva, Dr. F. Reiß, Prof. Dr. T. Beweries, Prof. Dr. A. Schulz
[b]Leibniz-Institut für Katalyse e.V., Albert-Einstein-Straße 29a, D-18059 Rostock, Germany.
[c] Dr. O. S. Bokareva, Department Life, Light & Matter, Universität Rostock, Albert-Einstein-Str. 3a, D-18059 Rostock, Germany

Abstract: Biradical(oid)s are key intermediates in the formation and cleavage of chemical bonds, and their application as molecular switches is of particular interest. In contrast, tetraradical(oid)s remain far less explored, although they may, for example, consist of two biradical(oid) units. Herein, we report the synthesis of phosphorus-centred bi- and tetraradicaloids coordinated to group 4 metallocene fragments of titanium and zirconium. The target compounds were obtained via ring-expansion reactions of metallocene-substituted isonitriles with one or two equivalents of the biradicaloid [˙P(μ-NTer)]$_2$, affording group 4 metallocene complexes bearing one or two bridged P-centred, five-membered heterocyclic biradicaloid units. These systems function as mono- and double-molecular switches, respectively, each based on a biradicaloid motif. Upon irradiation with light (638 nm), the biradicaloid heterocycles undergo transannular bond formation in one or both five-membered heterocyclic biradicaloid units, resulting in the generation of housane-type species. The photoinduced switching behaviour as well as CO_2 activation were investigated in solution by NMR and UV/Vis spectroscopy. Quantum-chemical calculations were further performed to examine the design of the isonitrile ligands, the mechanism of their insertion reactions, and the electronic structure and photoswitching behaviour, supporting the experimental findings.

Introduction

Heteroatom-centered biradical(oid)s have been extensively investigated due to their distinctive electronic structures and their ability to activate small molecules under mild conditions.[1–9] Selected examples (species **1**, **2**, **3**, **5** and **7**) are depicted in Scheme 1. In contrast, tetraradical(oid)s remain much less explored, largely because of their low stability, particularly in the case of “perfect” tetraradicals lacking magnetic coupling between radical centres.[1] Stabilization can be achieved when exchange interactions favour a singlet ground state, in which case the term tetraradicaloid is commonly used (e.g. species **6** and **8**). One important subclass comprises formal assemblies of two biradicaloid units, often referred to as bis(biradicaloids) (e.g., species **4** and **10**)[10,11] when inter-unit coupling is weak.[1] Moreover, coupling between radical centers within the two biradicaloid units of the tetraradicaloid can differ in nature. For example, in biradicaloid four-membered heterocycles **5** and **1**, transannular coupling may be either bonding or antibonding; the dominant biradical Lewis representation therefore features either a fractional single π bond (as in **5**, notation: •–•) or a fractional single π antibond (as in **1,** notation**:** •···•) between the transannular radical centers.[19]

Recently, phosphorus-centered tetraradical systems based on cyclopentane-1,3-diyl heterocycles – such as the bis(biradicaloid) **4** and the indacene-based tetraradicaloid **8** – have been reported, employing a non-conjugated linker in the former case and a conjugated linker in the latter.[10,12] Notably, biradicaloid compound **2,** generated by insertion of an isonitrile in one P-N bond in [˙P(μ-NTer)]$_2$ (**1**, Ter = terphenyl = 2,6-bis(2,4,6-trimethylphenyl)phenyl), undergoes reversible photoinduced transannular P–P bond formation to afford housane-type species **2h** (Scheme 1, top), analogous to the behaviour of the related formal tetraradical **4**, whereas no molecular switching has been observed for biradicaloid compounds **5** and **7** and their derived tetraradicaloids.[10,11,13,14]



Scheme 1. Selected known bi- and derived tetraradicaloids. *Notation*: •···• = π-antibond with biradical character, •–• = π-bond with biradical character.[19]

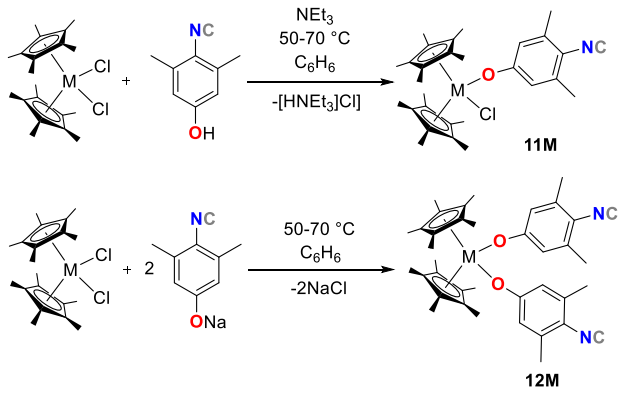
To date, tetraradical(oid)-based molecular switches incorporating transition-metal fragments remain extremely rare.[11] Incorporation of transition-metal units offers a powerful strategy to modulate the electronic properties of open-shell main-group systems by introducing metal-based *d* orbitals as well as steric and electronic ligand effects.[15] Although group 4 metallocenes in the +IV oxidation state are often considered photochemically inert, ligand-to-metal charge-transfer processes can induce photoactivity in selected systems.[16–18]Such hybrid transition-metal/main-group assemblies therefore hold considerable promise for light-controlled bond formation and cleavage.

Herein, we report the synthesis, characterization, and photo-switching behaviour of phosphorus-centered bi- and tetraradicaloid systems linked to group 4 metallocene fragments via a chemically inert metallocene phenoxy linker. Beyond the synthesis of bi- and tetraradicaloids connected to metallocene fragments, their electronic structure and switching behaviour, we also present a detailed exploration of the synthesis and design of the novel metallocene isonitriles, along with an in-depth discussion of the isonitrile insertion reaction that affords the biradicaloid five-membered heterocycle.

Results and Discussion

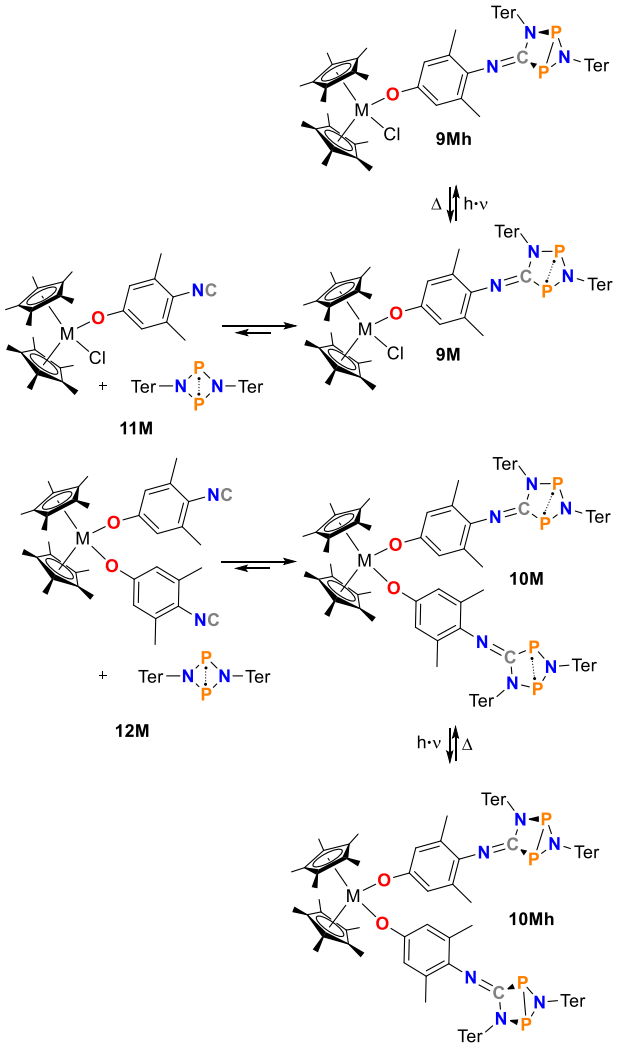
Synthesis – Design of the mono and double switch

To construct the metallocene-bridged P-centered biradicaloid or tetraradicaloid such as compound **9** and **10**, we envisaged exploiting the isonitrile insertion reaction as depicted in Scheme 1 (top). Therefore, to enable the incorporation of one and/or two biradicaloid switching units onto a metallocene scaffold, we first synthesized 4-isocyano-3,5-dimethylphenol and its sodium salt, which serve both as an isonitrile precursor and as a linker for subsequent attachment to the metallocene fragment (Scheme 2). The aryl 3- and 5-positions flanking the isonitrile functionality were blocked by methyl substituents, a modification that is essential to suppress undesired C–H activation at these sites during the formation of the targeted five-membered biradicaloids **9** and tetraradicaloids **10** (Scheme 1). Such C–H activation pathways are well documented and typically result in the formation of benzo-azaphospholes.[20] $Cp^*_2MCl_2$ (Cp^* = η^5-pentamethyl-cyclopentadienyl, M = Ti, Zr) was selected as the metallocene fragment because it is electron rich and can be coupled to the isonitrile aryl via salt metathesis reaction (Scheme 2).



Scheme 2. Synthesis of metallocenes bearing a phenoxy-isonitrile linker (M = Ti, Zr).

In an initial series of experiments, 4-isocyano-3,5-dimethylphenol and $Cp^*_2MCl_2$ were combined in a 1:1 ratio in benzene and heated to 60 °C, resulting in the formation of an intensely colored solution (Ti: red, Zr: green). Subsequent addition of Et_3N and stirring for three days, followed by recrystallization from THF (Ti) or toluene (Zr) at −78 °C, afforded crystalline material **11M** in good yields (M = Ti: 65%, M = Zr: 72%). Single-crystal X-ray diffraction (SC-XRD) analysis unambiguously confirmed the formation of the desired products (Figure 1), which is further supported by NMR and MS data as well as the presence of the characteristic C≡N stretching vibration at 2112 cm^{-1} (M = Zr) in the Raman experiment.



Scheme 3. Synthesis of metallocene-bridged P-centered biradicaloid (**9M**) and tetraradicaloid (**10M**) for M = Ti, Zr and their photoisomerization to the housane species **9Mh** and **10Mh** (h = housane).

For the synthesis of the diisonitrile complexes (**12M**), the protocol was slightly modified (Scheme 2, bottom). Instead of 4-isocyano-3,5-dimethylphenol, its sodium salt was employed, as this approach resulted in improved yields and reduced formation of side products. $Cp^*_2MCl_2$ and sodium 4-isocyano-3,5-dimethyl-phenolate were suspended in benzene at ambient temperature in a 1:2 molar ratio, and the mixture was stirred at ca. 60 °C for three days. The resulting red(Ti)/light-yellow(Zr) suspension was cooled to room temperature, filtered, and the residue was

extracted with fresh benzene. Recrystallization afforded **12M** in good yields (**12Ti**: 78%, **12Zr**: 82%). Both complexes were unambiguously characterized by SC-XRD analysis (Figure 2), NMR spectroscopy, as well as Raman and IR spectroscopy, exhibiting characteristic C≡N stretching vibrations at ν_{Raman}(C≡N) = 2111 (Ti) and 2113 cm^{-1} (Zr). Additional examples of titanocen-based isonitriles were synthesized and fully characterized but are not discussed here (see ESI).

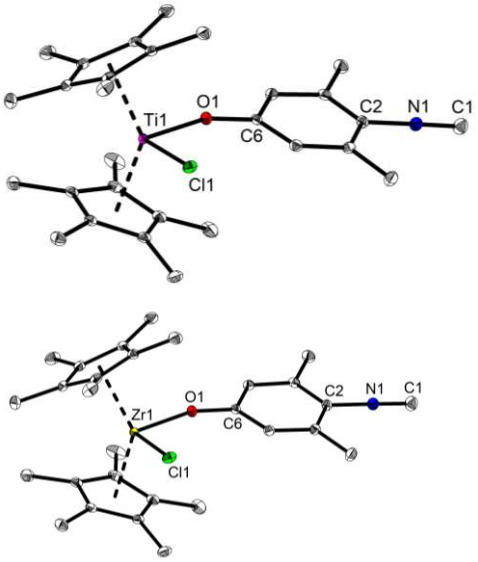


Figure 1. Molecular structure of complex **11Ti** (top) and **11Zr** (bottom) in the crystal. Thermal ellipsoids correspond to 30% probability (at 110 K for **11Ti** and 150 K for **11Zr**). Hydrogen atoms are omitted for clarity. Selected structural data (distances in Å, angles in °). **11Ti**: O1-Ti1 1.897(1), Cl1-Ti1 2.3780(4), C1-N1 1.160(2); O1-Ti1-Cl1 94.64(3), C6-O1-Ti1 158.6(1); **11Zr**: O1-Zr1 1.991(1), Cl1-Zr1 2.4644(4), C1-N1 1.155(2); O1-Zr1-Cl1 95.60(3), C6-O1-Zr1 161.5(1).

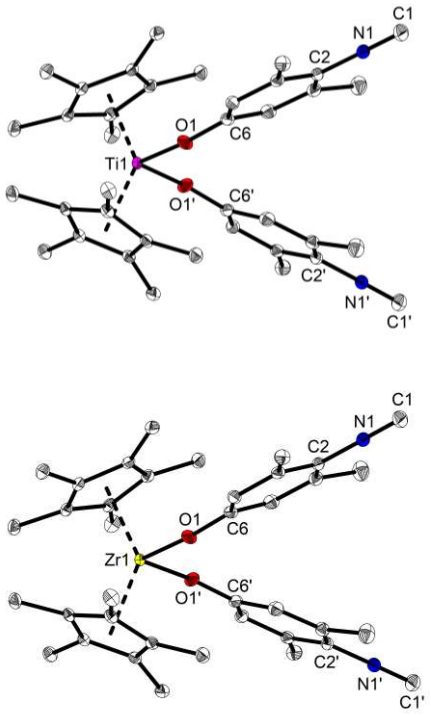


Figure 2. Molecular structure of complex **12Ti**·C_6H_6 (top) and **12Zr**·C_6H_6 (bottom) in the crystal. Thermal ellipsoids correspond to 30% probability (at 150 K for **12Ti** and 110 K **12Zr**). Hydrogen atoms and co-crystallized benzene are omitted for clarity. Selected structural data (distances in Å, angles in °). **12Ti**: O1-Ti1 1.929(1), C1-N1 1.158(2); O1-Ti1-O1' 98.78(7), C6-O1-Ti1 151.3(1), C6-O1-O1'-C6' 43.2(1); **12Zr**: O1-Zr1 2.018(1), C1-N1 1.155(2); O1-Zr1-O1' 98.02(7); C6-O1-Zr1-152.6(1), C6-O1-O1'-C6' 41.3(1).

Table 1. Characteristic analytical data (color, yield and ^{31}P NMR data) of **9M**/**9Mh** and **10M**/**10Mh**.

	9Ti	**9Zr**	**10Ti**	**10Zr**
color	green	green	green	green
λ_{max}[b]	658	657	654	656
yield [%]	85	71	65	70
δ[^{31}P]	261.5	261.8	261.5	262.0
	-	-	260.9	261.5
	227.2	226.5	228.2	227.7
	-	-	225.7	225.6
$\lvert {}^2J_{PP} \rvert$	148	147	143	146
	-	-	151	150
	9Tih	**9Zrh**	**10Tih**	**10Zrh**
color	colorless	colorless	colorless	colorless
δ[^{31}P]	−61.6	−62.3	−62.3[a]	−62.3
	-	-	−62.3[a]	−62.4
	−121.9	−123.6	−118.0[a]	−119.0
	-	-	−118.0[a]	−121.4
$\lvert {}^1J_{PP} \rvert$	70	71	-	71
	-	-	-	71

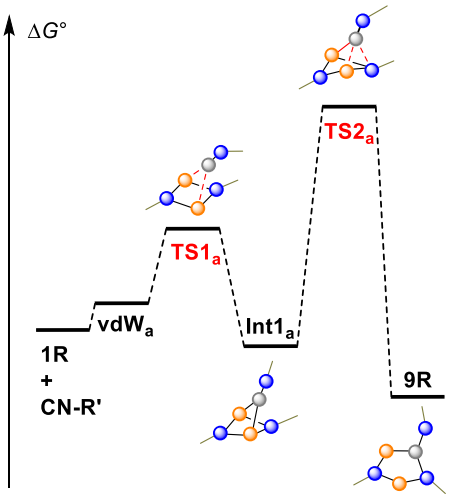
[a] A broad signal appearing as a multiplet. [b] in nm, only the λ_{max} value associated mainly with the HOMO–LUMO excitation is provided.

In a second series of experiments, we investigated the insertion reaction of the isonitrile-substituted metallocenes into biradicaloid **1** (Scheme 3). As these processes represent genuine equilibrium reactions, the isolation of either the pure biradicaloid **9M** or the tetraradicaloid **10M** proved challenging. Consequently, solutions invariably contained mixtures of biradicaloid **1** and **9M** or tetraradicaloid **10M**, along with the free isonitrile-functionalized metallocene complex. However, the equilibrium could be shifted significantly toward the insertion products by employing a two-fold excess of biradicaloid **1**.

In a typical experiment, the mono-isonitrile **11M** or diisonitrile complex **12M** and biradicaloid **1** were combined using a twofold excess of the latter and dissolved in benzene (Scheme 3). The resulting dark-green solution, characteristic of the formation of the five-membered biradicaloid,[11] was stirred at ambient temperature. After 30 min, the mixture was filtered, and all volatile components were removed under reduced pressure. Recrystallization followed by drying afforded the corresponding product as a green solid in good yields (Table 1).

The progress of the reaction could be readily monitored by ^{31}P NMR spectroscopy (Table 1): the resonance of **1** at ca. 276 ppm (singlet) gradually decreased (but never disappeared completely as this species was added in excess), while formation of the five-membered P-centered biradicaloid of type **9M** or **10M** gave rise to two new signals at ca. 260 ppm (doublet) and 226 ppm (doublet) with rather large P–P coupling constants (ca. 140–160 Hz). In

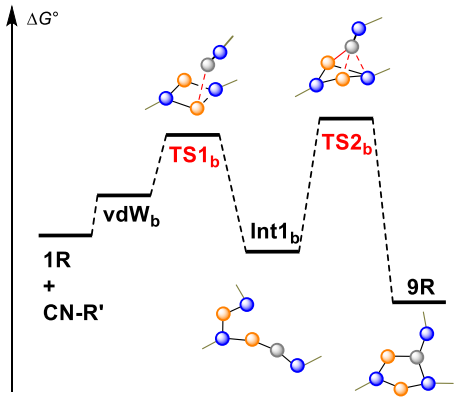
several cases, depending on sample stoichiometry and purity, additional resonances were detected within the expected chemical shift region. These signals are attributed to isonitrile-bridged species of **9M** and **10M** (i.e. the formal (2+1) addition products between the isonitrile and **9M** or **10M**) and consist of two doublets appearing in a similar range but exhibiting significantly smaller $^2J_{PP}$ coupling constants (5–50 Hz) compared with those observed for P-centered bi-/tetraradicaloids based on cyclopentane-1,3-diyl **2** (140–160 Hz, Scheme 1).[10,21]



Scheme 4. Schematic illustration of the reaction pathway a; detailed schemes including exact energies for each system are available in the ESI (Figures S38, S40, S42, S44, S46, S48). **vdW$_a$** refers to a van der Waals complex that forms when the isonitrile approaches biradicaloid **1**. Substituents not shown (see Table 2).

Mechanism of isonitrile insertion reaction

To probe the isonitrile insertion event, reaction pathways were computed using DFT followed by single-point DLPNO-CCSD(T) calculations (DLPNO-CCSD(T)/def2-TZVP//PBE-D3/def2-TZVP).[22–27] A first series employed the model system **1** + CN–R (no metal fragment but R = Me, CCl_3, Ph, 2,4,6-trichlorophenyl), while a second series retained the organometallic linker but replaced the terphenyl substituent in **1** with H. Two distinct mechanistic pathways for the approach of the isonitrile fragment to the biradicaloid precursor (**1**) were examined. In the first, symmetric pathway (a, Scheme 4), the isonitrile approaches both phosphorus atoms simultaneously, forming two P–C bonds in a concerted manner. Although this mechanism yields a thermodynamically stable intermediate product (**Int1$_a$**), the second transition state (**TS2$_a$**) is very high in energy, making the reaction kinetically challenging under standard conditions and likely requiring strong heating or alternative routes. In the second, unsymmetric pathway (b, Scheme 5), the CN(-R') group initially coordinates to a single phosphorus atom, forming an acyclic intermediate (**Int1$_b$**), before undergoing ring closure via a second, thermally accessible barrier (**TS2$_b$**). This stepwise mechanism exhibits a significantly lower overall barrier ($\Delta_{TS2b}G^{\ddagger} << \Delta_{TS2a}G^{\ddagger}$, Table 2) and is therefore the experimentally accessible route. This behaviour is consistent across all studied substituents R and R' (see ESI, Table 2, Figures S38–S49). The effect of the isonitrile substituent (R' in CNR') on both pathways and on product stability was also evaluated, with both mechanisms converging to the same five-membered product, allowing direct comparison of kinetic profiles and substituent influences. All insertion reactions are exergonic (−29 to −120 kJ mol^{-1}; Table 2), with electron-withdrawing substituents providing significantly enhanced stabilization of the five-membered biradicaloid. No significant differences are observed between the Ti and Zr species.



Scheme 5. Schematic illustration of the reaction pathway b; detailed schemes including exact energies for each system are available in the ESI (Figures S39, S41, S43, S45, S47, S49). **vdW$_b$** refers to a van der Waals complex that forms when the isonitrile approaches biradicaloid **1**. Substituents not shown (see Table 2).

Table 2. Computed activation and Gibbs free energies for the reaction of **1R** with CN–R' to form biradicaloid **9R** according to Schemes 4 and 5 (in kJ mol^{-1}, level of theory: DLPNO-CCSD(T)/def2-TZVP//PBE-D3/def2-TZVP, $c°$ = 1 mol/L).[c,d]

R = H R' =	$\Delta_{TS1a}G^{\ddagger}$	$\Delta_{TS2a}G^{\ddagger}$	$\Delta_{TS1b}G^{\ddagger}$	$\Delta_{TS2b}G^{\ddagger}$	$\Delta_rG°$
O[Ti][a]	70.6	228.2	50.2	137.6	-63.1
O[Zr] [a]	71.2	228.1	53.0	140.5	-62.3
R = Ter R' =	**$\Delta_{TS1a}G^{\ddagger}$**	**$\Delta_{TS2a}G^{\ddagger}$**	**$\Delta_{TS1b}G^{\ddagger}$**	**$\Delta_{TS2b}G^{\ddagger}$**	**$\Delta_rG°$**
Me	60.1	234.2	86.6	73.2	-29.1
CCl_3	97.2	119.5	86.8	33.2	-119.8
Ph	49.8	223.0	139.3	105.0	-56.7
TCP[b]	33.2	151.8	85.2	89.2	-65.3

[a] 4-isocyano-3,5-dimethylphenyl-Zr(cp*)$_2$, [b] TCP = 2,4,6-trichloro-phenyl, [c] pure DFT results are listed in Figures S40-S47, [d] All activation barriers and reaction energies were computed relative to the starting materials, which were defined as the zero-energy reference point.

Molecular structure of 9M/9Mh and 10M/10Mh

Attempts to obtain single crystals of **9M**/**9Mh** or **10M**/**10Mh** suitable for X-ray diffraction were unsuccessful, as neither solution nor solid samples could be rendered phase-pure owing to the underlying equilibrium chemistry (vide supra). As experimental structure data could not be obtained, all eight experimentally investigated systems (**9M**, **9Mh**, **10M**, and **10Mh**, M = Ti, Zr) were studied computationally at the DFT level of theory (PBE-D3/def2-TZVP). Initially, the isomeric space was explored using the CREST/CENSO workflow,[28,29] followed by a more detailed investigation of the thermodynamically favoured isomers (see ESI). The computed structures of the thermodynamically preferred bi- and tetraradicaloids (**9M** and **10M**), as well as their corresponding housane isomers (**9Mh** and **10Mh**), together with

selected metric parameters (Table 3), are shown in Figure 3 and Figure 4.

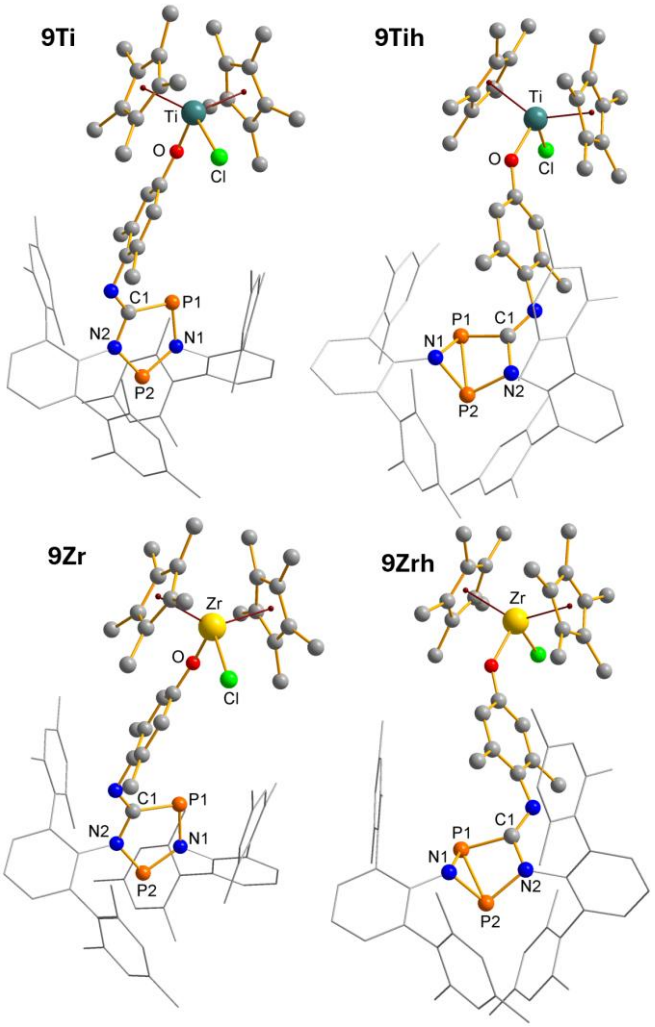


Figure 3. Ball-and-stick representation of the calculated structures (PBE-D3/def2-TZVP) for compounds **9M** (left) and **9Mh** (right). Ter-substituents are shown as wireframe. Selected structural data are listed in Table 3.

For the biradicaloid species **9M**, a *Z* conformation is found along the exocyclic C=N double bond between the five-membered heterocycle and the Ter-substituent (Figure 3), whereas for the tetraradicaloids **10M** (Figure 4) the calculations reveal that the thermodynamically most stable isomer adopts a *Z,Z* configuration, featuring two formal, heteroatom-substituted cyclopentane-1,3-diyl units, bridged by a metallocene fragment. As shown in Table 3, the structural parameters of the Ti and Zr biradicaloid units featuring five-membered phosphorus heterocycles are essentially identical, as are those of the corresponding tetraradicaloids. These observations indicate that the metal fragment exerts little to no influence on the structure of the five-membered heterocycles; rather, the terphenyl substituents are sufficiently flexible to form a molecular pocket that enables optimal accommodation of the five-membered ring. Both biradicaloids **9M** and tetraradicaloids **10M** contain one or two planar five-membered P_2N_2C heterocycles, respectively. These rings exhibit significantly shortened P–N bond lengths (1.678–1.742 Å; cf. Σr_{cov}(P–N) = 1.82 Å, Σr_{cov}(P=N) = 1.62 Å),[30] indicative of partial double-bond character and consistent with reported experimental metric parameters for related compounds such as **3** and **4**.[10] The transannular P···P separation (2.975–2.979 Å) is substantially longer than expected for a covalent P–P bond in line with its description as a π-antibond (vide supra, Scheme 1), yet markedly shorter than the sum of the van der Waals radii (Σr_{vdW}(P···P) = 3.80 Å).[31] Upon photochemical generation of the housane isomers **9Mh** and **10Mh** (vide infra), the computations predict the formation of a covalent P–P single bond (2.194–2.198 Å, cf. e.g., 2.177 Å in **3** for R = Dmp = dimethylphenyl[10] and Σr_{cov}(P–P) = 2.22 Å), accompanied by a pronounced pyramidalization of the nitrogen atom within the former PNP unit. Consequently, these housanes feature a three-membered ring fused to an almost perpendicularly oriented four-membered heterocycle. This structural motif is characterized by a bent P–P σ bond, P–N single bonds (1.787–1.817 Å), and a localized exocyclic C=N–R double bond which remains almost unchanged.

Table 3. Computed electronic data (PBE-D3/def2-TZVP) and selected structural parameters [distances in Å, angles in °] for biradicaloids **9M** and tetraradicaloids **10m** and their housane isomers **9Mh** and **10Mh**.

biradicaloid	**9Ti**[e]	**9Zr**[e]	**9Tih**[e]	**9Zrh**[e]
β[a]	31%	31%	5%	5%
$\Delta G°$[b]	–53.8	–50.9	–22.2	–20.7
$\Delta E_{S\text{-}T}$[c]	88.0	87.9	182.1	214.9
n[d]	0.31	0.31	0.05	0.05
P-P	2.977	2.979	2.198	2.194
P1-N1	1.741	1.742	1.809	1.817
P2-N1	1.684	1.684	1.787	1.795
P1-N1-P2	120.8	120.8	75.3	74.8
DE$\sphericalangle_{ring}$[g]	–0.8	–0.7	74.7	75.4
tetraradical	**10Ti**[f]	**10Zr**[f]	**10Tih**[f]	**10Zrh**[f]
β[a]	0.29	0.28	0.05	0.05
$\Delta G°$[b]	–122.8	–119.8	–44.8	–36.8
$\Delta E_{S\text{-}T}$[c]	108.5	109.2	166.0	199.9
n[d]	0.29	0.28	0.05	0.05
$n+1$[d]	0.29	0.28	0.05	0.05
P-P	2.975	2.975	2.198	2.194
P1-N1	1.737	1.736	1.816	1.814
P2-N1	1.678	1.678	1.789	1.787
P1-N1-P2	121.2	121.2	75.1	75.1
DE$\sphericalangle_{ring}$[g]	–1.0	–0.4	–75.0	–74.9

[a] $\beta = \frac{2c_2^2}{c_1^2+c_2^2}$, [b] Gibbs energy in kJ mol^{-1} ($c°$ = 1 mol/L) of the isonitrile insertion reaction: **11M** + **1** → **9M** (biradicaloid) or **12M** + **1** → **10M** (tetraradicaloid), [c] vertical singlet-triplet gap in kJ mol^{-1}, [d] occupation number of LUNO (lowest unoccupied natural orbital) as well as n+1 = occupation number of LUNO+1, [e] see Figure 3, [f] see Figure 4 - data provided for only one of the two five-membered rings, [g] DE = dihedral angle: ∢(P1-N1-P2-N2).

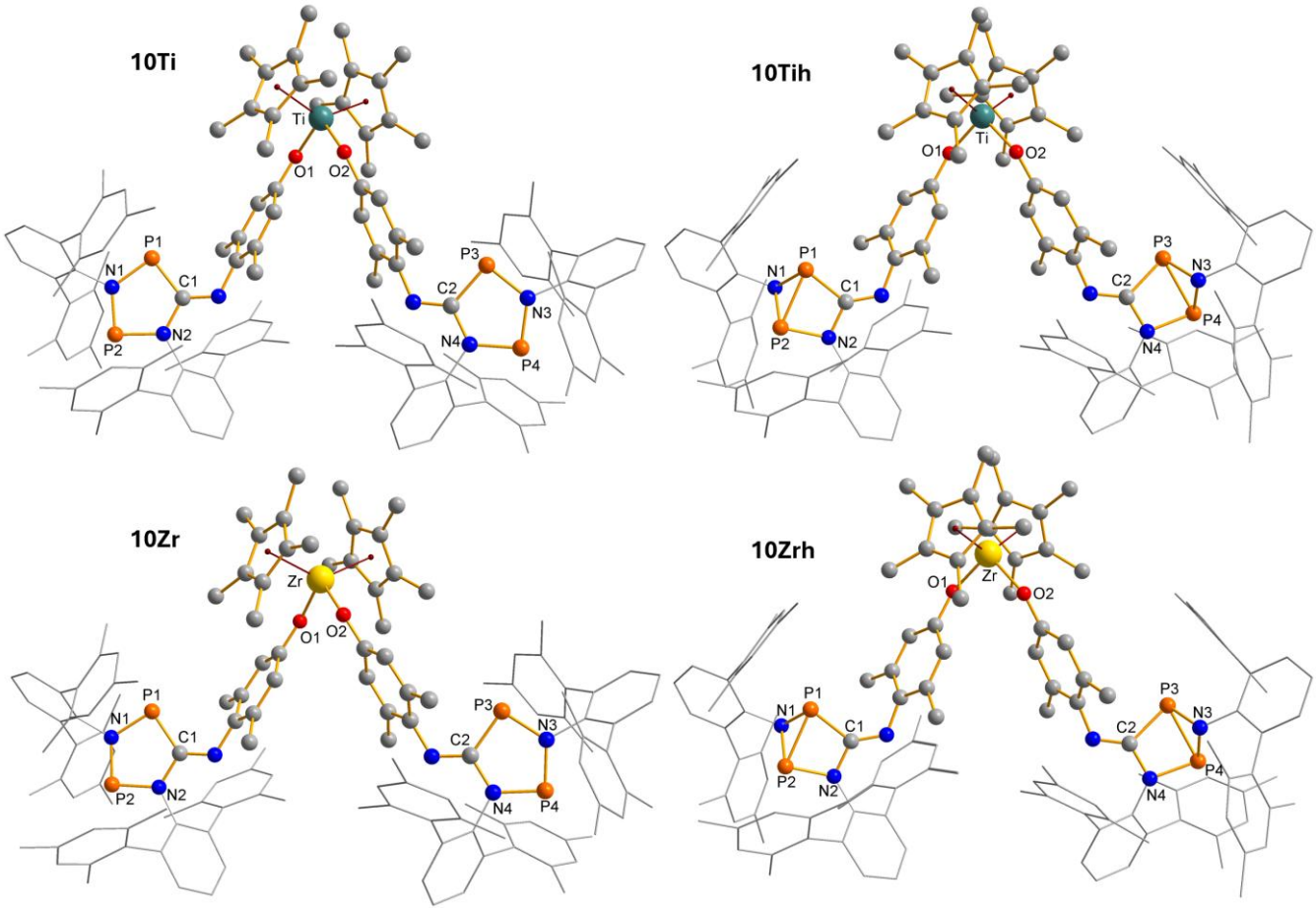


Figure 4. Ball-and-stick representation of the calculated structures (PBE-D3/def2-TZVP) for compounds **10M** and **10Mh**. Ter substituents shown as wireframe. Selected structural data are listed in Table 3.

Electronic structure of 9M/9Mh and 10M/10Mh

DFT calculations at the PBE-D3/def2-TZVP level of theory predict a singlet (^{1}A) ground state for all bi- and tetraradicaloid species, consistent with the absence of an EPR signal and the observation of sharp ^{31}P NMR resonances. The corresponding triplet states lie significantly higher in energy, with vertical singlet–triplet gaps ($\Delta E_{S\text{-}T}$) of approximately 88 kJ mol^{-1} (for **9Ti** and **9Zr**), whereas the housane species exhibit much larger singlet–triplet gaps of ca. 182 (**9Tih**) and 215 (**9Zrh**) kJ mol^{-1} (Table 3).

To assess the open-shell character of the singlet state in terms of biradical and tetraradical contributions, CASSCF(2,2) calculations were performed for the biradicaloids (Figure 5), whereas CASSCF(4,4) calculations were carried out for the tetraradicaloids (CASSCF = complete active space self-consistent field, Figure 6). The dominant contributions to the configuration interaction wave function of the ^{1}A state can be expressed as (coefficients c_1 and c_2, see Table S8):

$$\Psi_{\mathrm{CAS}(2,2)} \approx c_1 \mid 2,0\rangle + c_2 \mid 0,2\rangle.$$

A convenient measure of the biradical character is given by $\beta = 2c_2^2/(c_1^2 + c_2^2)$,[32] yielding values of 31% for **9Ti** and **9Zr** (cf. [(*μ*-NTer)P]$_2$ (**1**): 25%).[33–35]

Thus, insertion of the isonitrile into the four-membered ring of **1** preserves the biradical character, which is even slightly increased. Consistently, the natural orbital occupation numbers ($n_{(\mathrm{LUNO})}$ = 0.31, Table 3) clearly indicate significant open-shell singlet biradical character.[1] The biradical character of the housane species is very small (ca. 5%) and is therefore more appropriately attributed to dynamic electron correlation.

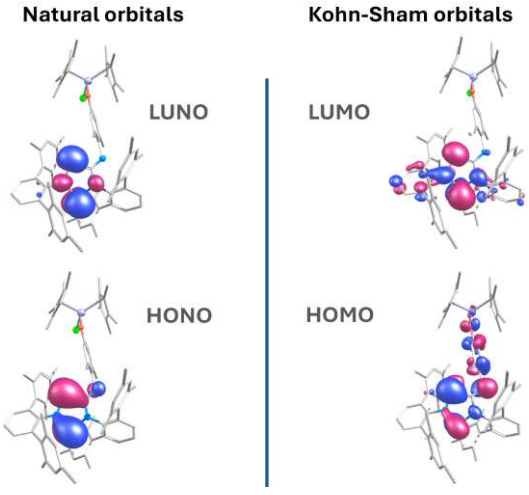


Figure 5. Left: CASSCF(2,2) orbitals; right: Kohn–Sham orbitals for **9Ti**. The corresponding orbitals for **9Zr** are similar (see Figure S52).

According to CASSCF(4,4) calculations, the ground state of the tetraradicaloid is also an open-shell singlet, separated from the corresponding triplet and quintet states by sizable energy gaps (ΔE_{S-T} = 109 kJ mol^{-1}, ΔE_{S-Q} = 199-200 kJ mol^{-1}, Table 3, Tables S18-S19, level of theory: PBE-D3/def2-TZVP). As observed for the structural parameters (see above), the biradical character of **10M** is close to that of the biradicaloids **9M** (28 - 29%), with no significant difference between **10Ti** and **10Zr**. This indicates that the metal fragment and the catenation have little influence on the biradical/tetraradical character. The identical occupation numbers of the LUNO/LUNO+1 (**10Ti**: 0.29e/0.29e; **10Zr**: 0.28e/0.28e) and HONO/HONO–1 (**10Ti**: 1.71e/1.71e; **10Zr**: 1.72e/1.72e) further confirm negligible coupling between the two five-membered heterocycles (LUNO = lowest unoccupied natural orbital; HONO = highest occupied natural orbital; **Figure 6**). Consistent with this, the biradical character of each unit (**10Ti**: 29%; **10Zr**: 28%) equals the overall tetraradical character (**10Ti**: 29%; **10Zr**: 28%), indicating the absence of electronic communication between the two biradical moieties. This behaviour is attributed to the extended bridging unit, which produces quasi-degenerate orbitals localized on each ring, and to disruption of π-delocalization by the metal fragment (Figure 6). Consequently, exchange coupling is effectively zero, and **10M** is more appropriately described as a bis(biradicaloid) rather than a tetraradicaloid.[1]

MO and NBO analyses of the biradical moieties in **9M**/**10M** reveal a delocalized 6π-electron system with polarized P–N bonds. The frontier Kohn-Sham orbitals (Figure 5) display classic biradicaloid features: the LUMO is (π-)bonding at the P centres but (π-)antibonding across the N–P–N–P moiety, while the HOMO is antibonding between P atoms and bonding along P–C–N and P–N. Population of the LUMO promotes a transannular P···P bonding interaction, leading to housane formation, in agreement with experiment (vide supra). This orbital-driven behaviour is characteristic of biradicaloid-based molecular switches (vide infra).[1,12] Finally, for all bi- and tetraradicaloid systems studied here, localization reveals a predominantly P-centered character. For clarity, the tetraradicaloid case is shown here only for **10Ti** as a representative example (**Figure 6**), consistent with the CASSCF occupation numbers and the quasi-degenerate orbitals in the delocalized representation.

Photoswitching – housane formation

As illustrated in Scheme 3, the metallocene-functionalized bi-/tetraradicaloids **9M** and **10M** are prone to photochemical isomerization to the corresponding [2.1.0] bicyclic housane species **9Mh** and **10Mh**. Thermal formation of the housane is precluded by the high activation barrier (e.g. **9Ti**: 114 and **9Zr**: 110 kJ mol^{-1}), whereas the reverse process is thermally accessible (**9Ti**: 84, **9Zr**: 79 kJ mol^{-1}).[21] Both species exhibit a characteristic deep-green color ($\lambda_{max} \approx$ 650–660nm, Table 1), with the dominant absorptions assigned to π → π transitions on the basis of time-dependent density functional theory (TD-DFT) calculations (see Figures S58, S60, S62, S63). Accordingly, irradiation with red light promotes excitation to the S_1 state, from which the excited species can either relax back to the bi-/tetraradicaloid ground state via a conical intersection or convert to the housane isomers with an estimated probability of ca. 25%. As there is minimal influence of the transition-metal fragments on the electronic structure of the five-membered heterocycles, and the biradical sites of each ring exhibit negligible electronic coupling, the photoswitching behavior closely resembles that of the corresponding metal-free five-membered heterocycle described previously.[21] Therefore, no further discussion is provided here, as the focus is on the switching process and activation chemistry.

The biradicaloid–housane interconversion can be conveniently monitored by UV/Vis and ^{31}P NMR spectroscopy, both under irradiation and in the dark.

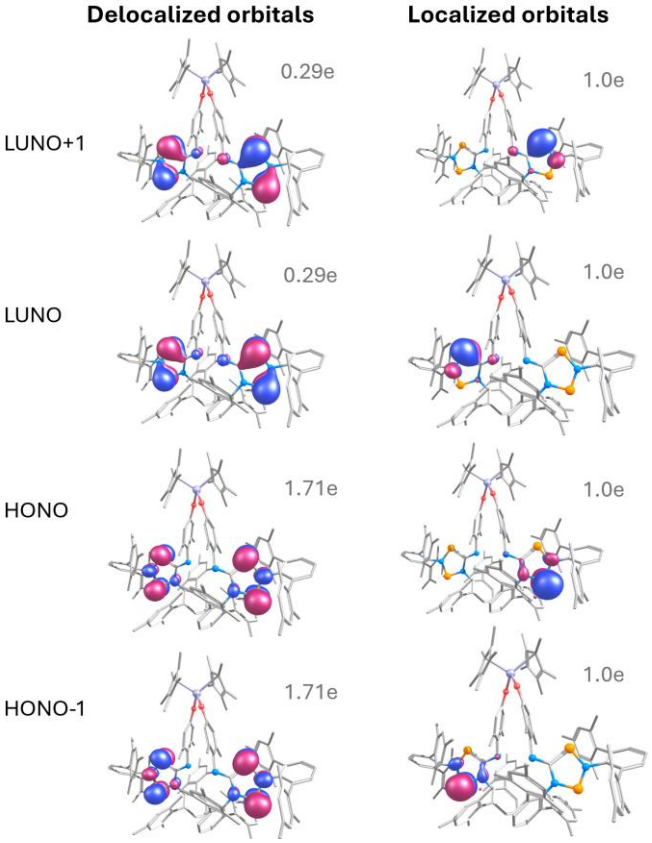


Figure 6. CASSCF(4,4) natural orbitals for **10Ti** with occupation numbers (left) and their localized counterparts (right). The analogous orbitals for **10Zr**, which are visually similar, are provided in the Supporting Information (Figure S56).

UV/Vis study: In the absence of irradiation, the UV/Vis spectrum displays two absorption maxima at ca. 650–660 and 440–450 nm (Figure 7), in good agreement with the computed spectra (see ESI). In particular, the absorption at ca. 650 nm, which originates essentially from a HOMO → LUMO transition (e.g. for **9Ti** in Figure 5), serves as a diagnostic signature for the biradicaloid species.

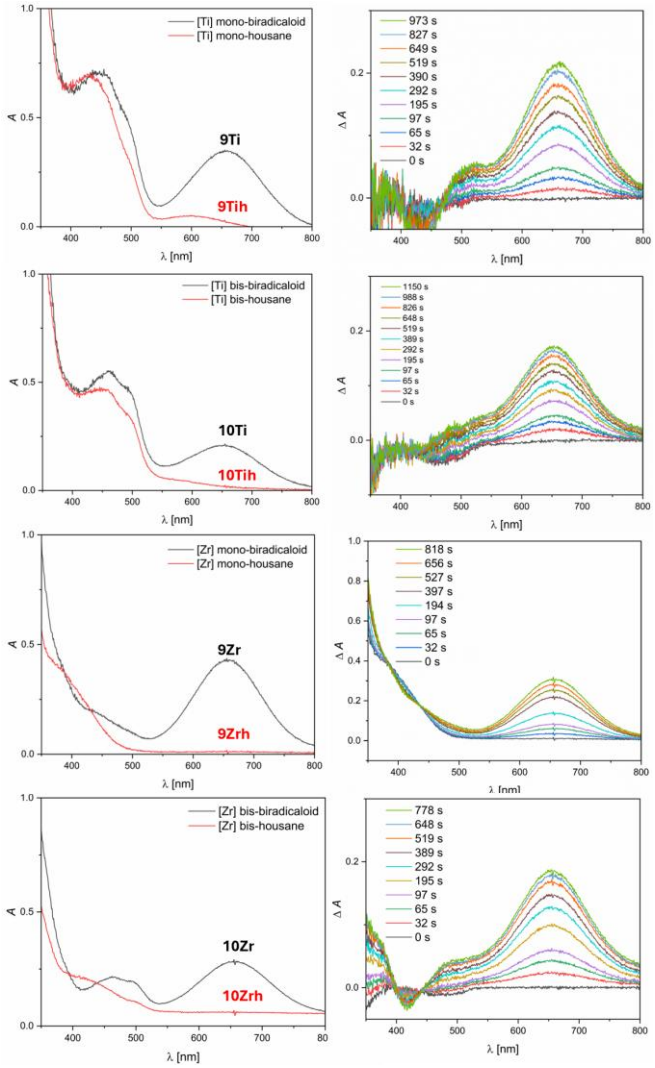


Figure 7. UV/Vis spectra recorded in the presence and absence of irradiation. **Left:** Photoisomerization of the photoswitch (570 nm filter) from complexes **9M**/**10M** to the corresponding housane-type complexes **9Mh**/**10Mh**. **Right:** Investigation of the thermal reverse reaction at 20 °C. Irradiation at 570 nm converts the biradicaloid species into the housane structure, after which a blank measurement and time-resolved UV/Vis spectra were recorded. The spectra shown represent selected time points. The gradual increase of the characteristic biradicaloid absorption band at ca. 650–660 nm provides direct evidence for the thermal back-reaction.

This transition can be understood as the excitation of an electron from the transannular P···P π-antibond into the unoccupied π-bond (vide supra), rendering this wavelength well suited to trigger the photoisomerization process. The second absorption band observed between 400 and 500 nm is assigned to the HOMO−1 → LUMO transition, which likewise increases population of the transannular P···P bonding orbital. These electronic excitations rationalize the efficient photochemical conversion of the biradicaloid species **9M**/**10M** into the corresponding housane isomers **9Mh**/**10Mh**, as population of the LUMO promotes formation of the transannular P···P bond characteristic of the housane-type bicyclic structure (Figure 3, Figure 4).

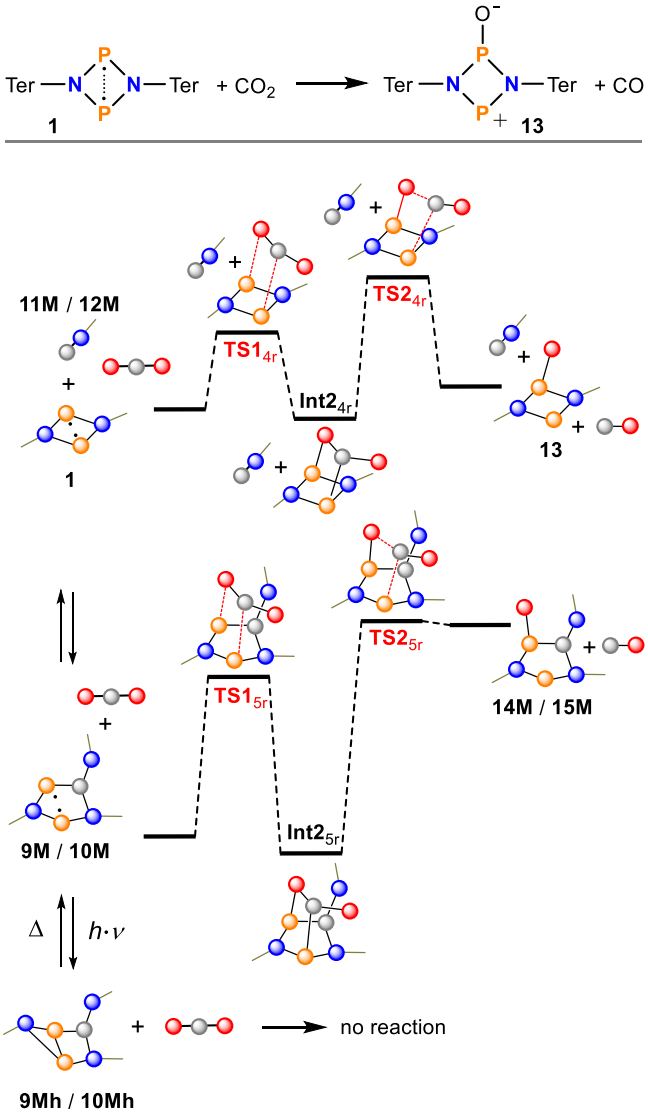
Accordingly, irradiation at 570 nm during the UV/Vis measurement initially yields UV–vis spectra exclusively attributable to the housane species (Figure 7, and Figures S17-S20). Upon cessation of irradiation, thermal equilibration enables the reverse isomerization, regenerating the heterocyclic 1,3-diyl biradicals, as evidenced by the gradual increase of the characteristic biradical absorption band at ca. 655 nm. This observation provides direct spectroscopic proof for the thermally accessible reverse reaction. After approximately 20 min, no housane species could be detected, and only the biradicaloid or bis(biradicaloid) forms **9M**/**10M** remained. No decomposition was observed.

^{31}P NMR study: As summarized in Table 1, irradiation induces a pronounced high-field shift in the ^{31}P NMR spectra (Δδ > 250 ppm) upon formation of the housane species. Whereas the bi-/tetraradicaloid species **9M**/**10M** display two doublets in the range δ(^{31}P) = +262 to +143 ppm, the corresponding housane isomers **9Mh**/**10Mh** resonate markedly upfield at −61 to −124 ppm (Table 1). Concomitantly, a significant reduction of the P–P coupling constants is observed ($|J_{PP}|$ = 143–148 Hz for **9M**/**10M** vs 70–71 Hz for **9Mh**/**10Mh**), in agreement with previously reported experimental data and computed values (see ESI).[12] As shown in Figure S21-S27, in the absence of irradiation only the two low-field doublets at ca. 260 and 140 ppm are detected, consistent with the exclusive presence of the biradicaloid or bis(biradicaloid) species. In contrast, irradiation of the NMR sample *in situ* with red laser light (638 nm) results in almost complete conversion to the housane species, as evidenced by the appearance of the corresponding high-field signals. Upon switching off the light source, the bi-/tetraradicaloid species **9M**/**10M** are fully regenerated within 25 min, accompanied by the complete disappearance of the housane resonances. It should be noted that, owing to the equilibrium between **9M**/**10M** ⇌ **1** + R'NC, the ^{31}P NMR resonance of the four-membered biradicaloid **1** (singlet at 276 ppm) is observed throughout; its intensity, however, also diminishes upon irradiation.

Photoswitchable On–Off Control of CO_2 Activation

To probe the ability of **9M**/**10M** to activate CO_2, the gas was introduced into a THF solution of the bi-/tetraradicaloid species under exclusion of light at ambient temperatures. The reactions were carried out using **9Ti** and **10Zr** as representative examples. Reaction progress was monitored by ^{31}P NMR spectroscopy (**9Ti**: Figure 8, **10Zr**: Figures S29-S30; Scheme 6). Within minutes after a short induction period, the initially green solution developed an intense red coloration, concomitant with the appearance of a new product characterized by an AB spin system at δ[^{31}P] = 335.0 and 196.6 ppm with $^2J_{PP}$ = 52 Hz. Simultaneously, the diagnostic doublet resonances of **9M**/**10M** at ca. 260 and 227 ppm (Table 1) vanished. *Note*: The signal at δ[^{31}P] = 276 ppm for **1** is absent from the outset, and only the five-membered biradicaloid moieties are observed. The use of an excess of one equivalent of RNC shifts the equilibrium almost completely toward the five-membered biradicaloid, rendering the four-membered biradicaloid undetectable. In addition, compound **1**, once formed, is rapidly consumed by reaction with CO_2, ultimately affording **13** and CO. The newly formed species (δ[^{31}P] = 335.0 and 196.6 ppm) is assigned to the partially oxidized, literature-reported compound [OP(*μ*-NTer)$_2$P] (**13**, Scheme 6, Figure 8),[36] which is known to arise from exposure of biradicaloid **1** to CO_2. Given the dynamic equilibrium between the five-membered biradicaloid **9M**/**10M** and the four-membered biradicaloid **1**, the latter is continuously generated and selectively scavenged by CO_2. This irreversible trapping effectively removes **1** from the equilibrium, thereby driving quantitative conversion of **9M**/**10M** via **1** to the final product **13** within 9h in the case of **9Ti** (Figure 8; **10Zr**: 24h, Figure S30). The formation of CO was unambiguously confirmed by gas-phase

IR spectroscopy (ν_{CO} = 2139 cm^{-1}, cf. 2344 cm^{-1} for CO_2, Figure S36) and ^{13}C NMR spectroscopy (184 ppm, cf. 126 ppm for CO_2 in C_6D_6, Figure S37).



Scheme 6. Top: Literature known CO_2 activation by biradicaloid **1**.[36] Bottom: Simplified schematic representation of the equilibrium chemistry between the four-membered biradicaloid **1** + R'NC (**11M**/**12M**), **9M**/**10M**, and their corresponding housane species **9Mh**/**10Mh** in reactions with CO_2. Color code: oxygen (red), nitrogen (blue), carbon (grey), and phosphorus (orange). Under irradiation, the equilibrium is shifted almost exclusively toward housane formation, thereby suppressing CO_2 activation. Upon cessation of light, the four-membered biradicaloid **1** efficiently activates CO_2, as the barrier for **TS1$_{4r}$** is significantly lower than that for **TS1$_{5r}$**. Consequently, **13** is formed exclusively, in agreement with ^{31}P NMR spectroscopic data. The exact data for the various species **9M**/**10M** can be found in the ESI (Figures S66-S70). *Note:* All activation barriers and reaction energies were computed relative to the starting materials, which were defined as the zero-energy reference point. Moreover, $\Delta_{TS2,5r}G^{\ddagger}$ = could not be found, but since the reaction is highly endergonic (>115 kJ mol^{-1}), it can be assumed that it lies well above 115 kJ mol^{-1}. This means it cannot be overcome at room temperature, i.e., **14M**/**15M** does not form because it is thermodynamically too unfavourable.

These experimental observations are fully consistent with DFT calculations (PBE-D3/def2-TZVP), which predict a substantially higher activation barriers for direct reaction of **9M**/**10M** with CO_2 ($\Delta_{TS1,5r}G^{\ddagger}$(**9Ti**) = 45.1 and $\Delta_{TS2,5r}G^{\ddagger}$(**9Ti**) = >114.5 kJ mol^{-1}) relative to CO_2 activation by biradicaloid **1** ($\Delta_{TS1,4r}G^{\ddagger}$(**1**) = 30.8 and $\Delta_{TS2,5r}G^{\ddagger}$ (**1**) = 91.3 kJ mol^{-1}, Scheme 6, Figure S66). The intermediates **Int2$_{4r}$** and **Int2$_{5r}$** were not observed experimentally. Furthermore, formation of **14M**/**15M** is calculated to be highly endergonic (e.g. **14Ti**: 83.6, **14Zr**: 83.7 kJ mol^{-1}), whereas formation of **13** (+16 kJ mol^{-1}) is only slightly endergonic, underscoring also the thermodynamic preference for CO_2 activation via the four-membered biradicaloid pathway (Figures S66-S70). The concomitant generation of carbon monoxide was experimentally verified (vide supra, see ESI).[37] *Note:* Although $\Delta_{298}G^{\circ}$(**1**+CO_2 → **13**+CO) is slightly positive (+16 kJ mol^{-1}), the reaction proceeds under non-standard conditions because continuous removal of gaseous CO lowers its partial pressure, thereby shifting the equilibrium toward products and rendering ΔG negative.

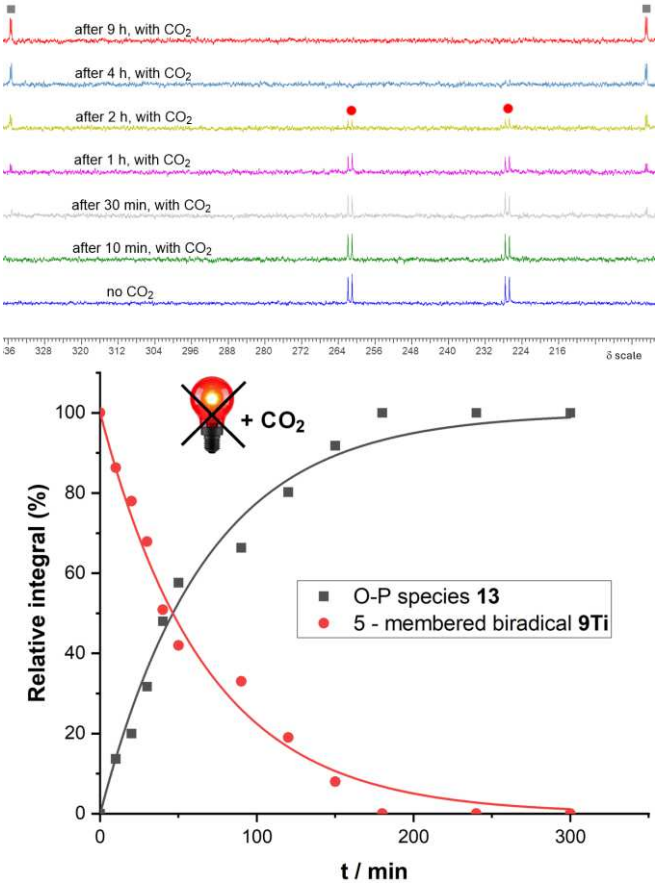


Figure 8. CO_2 is activated by the five-membered biradicaloid **9Ti**, which first equilibrates to the four-membered ring capable of CO_2 activation, ultimately yielding the PO-species **13** and CO. Top: Time-resolved ^{31}P NMR spectra. Bottom: Relative intensities of the five-membered biradicaloid **9Ti** (red dots) and the PO-product **13** (grey squares). Data were fitted using a pseudo-first-order model. Experimental data for double switch **10Zr** are depicted in the ESI.

Finally, an experiment was designed to assess the effect of irradiation on CO_2 activation and to determine whether this process can be suppressed via light-induced housane formation (**9Mh**/**10Mh**), as outlined in Scheme 6. To this end, two reaction vessels containing identical amounts of **9Ti** dissolved in THF were prepared. One sample was irradiated with red light (λ = 638 nm),

while the second sample was kept in the dark as a control (Figure 8). The ^{31}P NMR control experiment was already described in the previous section.

Irradiation-induced CO_2 activation opens an additional reaction pathway by incorporating the housane, thereby altering the equilibrium landscape (**Scheme 6**). The experiment was initiated in the dark in the absence of CO_2, showing exclusively the five-membered biradicaloid in the ^{31}P NMR spectrum (doublets at 262 and 227 ppm, spectrum A in Figure 9). Upon irradiation (λ = 638 nm), still in the absence of CO_2, only the housane species is observed after 20min (two doublet species at –62 and –122 ppm, spectra B-D, Figure 9). After the addition of CO_2, irradiation was continued for 2 h, with ^{31}P NMR spectra recorded every 30 min. As long as light of λ = 638 nm is applied, CO_2 activation is completely suppressed (Figure 9, spectrum E), as the equilibrium between the four-membered (276 ppm), five-membered (262 and 227 ppm), and housane species shifts entirely toward the housane (–62 and –122 ppm). In this species, a transannular P–P bond is present, resulting in a nearly negligible biradical character. Consequently, a closed-shell species is formed that is incapable of activating CO_2. Upon cessation of irradiation after 2 h, the system undergoes an almost instantaneous reversion to the five-membered biradicaloid (spectrum F), which only slowly equilibrates to the four-membered biradicaloid. After approximately 2 h in the dark, CO_2 activation proceeds (spectrum G), analogous to the control reaction conducted in the absence of light, as demonstrated by the rise of the two new signals at 335 and 197 ppm indicative for the formation of **13** (vide supra). These observations demonstrate that the molecular biradicaloid-housane switch can be used to reversibly toggle CO_2 activation. It should be noted that irradiation generates different isomeric mixtures compared to the dark reaction, leading to minor shifts in spectroscopic signals.

Conclusion

In summary, we report the synthesis of phosphorus-centered mono and bis(biradicaloid) complexes attached to group 4 metallocene fragments of zirconium and titanium. These target compounds were accessed via ring-expansion reactions of metallocene substituted isonitriles with one or two equivalents of [·P(μ-NTer)]$_2$ (**1**), affording group 4 metallocene complexes bearing one or two bridged P-centered biradicaloid five-membered heterocycles, respectively. While the isonitrile precursors were fully characterized, comprehensive characterization of the resulting biradicaloids **9M** and tetraradicals **10M** proved challenging due to pronounced equilibrium chemistry, in which partial reversion to the parent isonitrile and the four-membered biradicaloid **1** invariably occurs. Nevertheless, the presence of these species in solution was unambiguously established by NMR und UV/Vis spectroscopic studies. The resulting complexes operate as mono- and double-molecular switches based on the biradicaloid five-membered heterocyclic motif. Upon irradiation with visible light (λ = 638 nm), these biradicaloid heterocycles undergo transannular bond formation in one or both biradicaloid units, giving rise to housane-type species (**9Mh**/**10Mh**). This photoinduced switching behaviour, as well as the activation of CO_2, was demonstrated in solution by a combination of ^{31}P NMR and UV/Vis spectroscopy. Notably, CO_2 activation proceeds exclusively via the four-membered biradicaloid **1**, which is continuously present due to the delicate equilibrium with the five-membered metallocene-functionalised biradicaloid or bis(biradicaloid) species **9M**/**10M**, whereas direct activation by the latter is not observed.

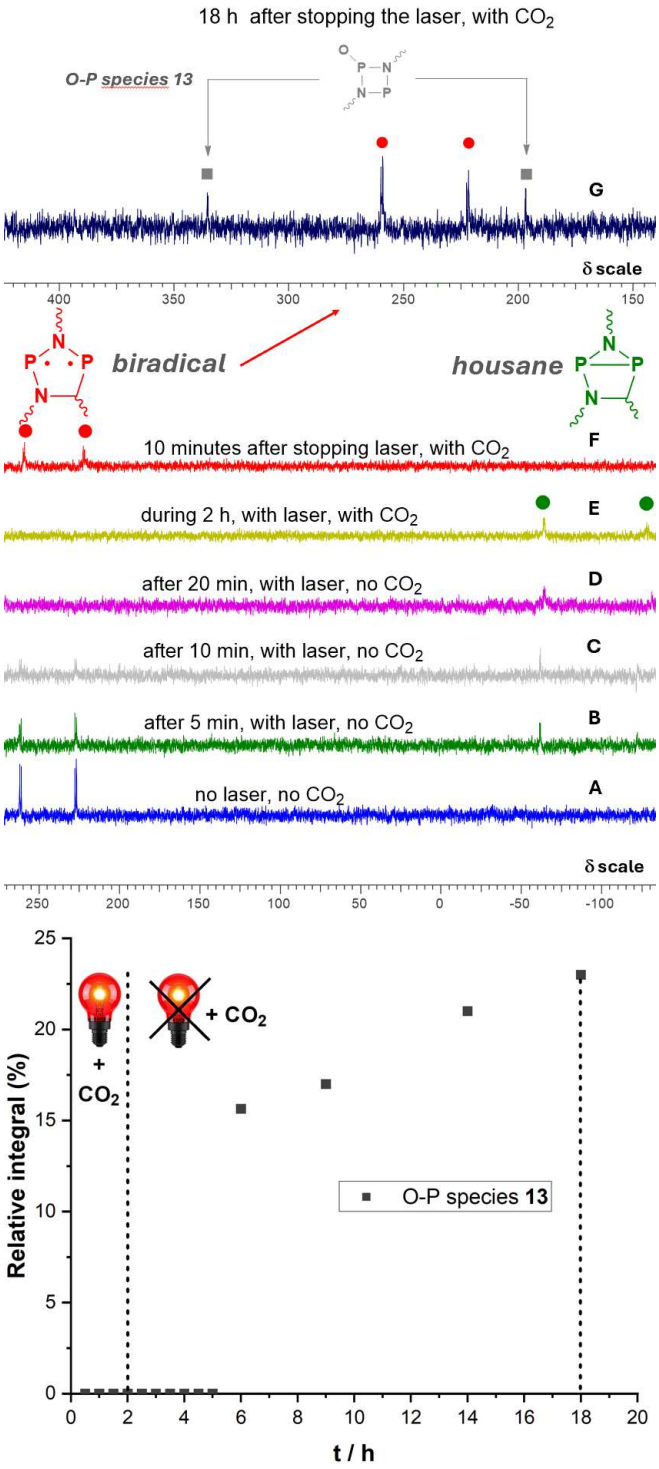


Figure 9. The molecular biradicaloid/housane **9Ti** / **9Tih** switch reversibly controls CO_2 activation. In the dark, the five-membered biradicaloid is observed by ^{31}P NMR (shown the relative integrals of **13**). Irradiation converts it to housane, suppressing CO_2 activation, which resumes only after the light is turned off as the housane reverts to the biradicaloid and equilibrates to the four-membered species. Top: Time-resolved ^{31}P NMR spectra. Bottom: Relative intensities of the PO-product **13** as a function of time.

No discernible metal effect (Ti vs Zr) on the (electronic) structure and no significant differences between the biradicaloid mono-switches **9M** and the corresponding double-switch systems **10M** were observed. This behaviour can be rationalized by theoretical considerations, which indicate that the long organometallic bridge effectively suppresses electronic communication between the two five-membered biradicaloid units in the formal tetraradicaloid species. Consequently, these compounds are more appropriately described as *bis(biradicaloids)* rather than true tetraradicaloids. Since **9M** and **10M** do not differ in their switching behaviour, but **9M** can be functionalized or reduced at the metal–Cl bond, we plan to investigate this system more closely in this regard in future studies.

Complementary quantum-chemical calculations provided mechanistic insight into the ligand design, the isonitrile insertion process and the electronic structure. These studies indicate that electron-withdrawing isonitrile substituents enhance the thermodynamic stability of the radical species **9M** and **10M**. Moreover, the insertion of the isonitrile was found to proceed via an unsymmetric pathway involving selective attack of only one phosphorus center and formation of an acyclic intermediate in an overall exergonic process. Collectively, these findings establish group 4 metallocene-supported P-centered biradical(oid)s as a versatile platform for switchable reactivity and small-molecule activation, governed by subtle equilibrium effects and external stimuli.

Experimental Section

All manipulations were carried out under oxygen- and moisture free conditions under argon using standard Schlenk or glovebox techniques at room temperature [298(3) K] unless noted otherwise. Removal of volatile substances *in vacuo* was carried out at 1×10^{-3} mbar. Further information on experimental procedures, preparation of starting materials, data acquisition and processing, purification procedures and a full set of analytical data for each compound as well as further details on the computations can be found in the **Supporting Material (ESI)**.

Associated Content

Supporting Information

The Supporting Information is available free of charge.

Experimental section, preparation of starting materials and compounds, structure elucidation, additional NMR and UV-vis spectra as well as computational details (PDF) along with Xyz-files of optimized structures (ZIP).

Accession Codes

CCDC 2505219 - 2505225 contain the supplementary crystallographic data for this paper. These data can be obtained free of charge: www.ccdc.cam.ac.uk/data_request/cif, or by emailing data_request@ccdc.cam.ac.uk, or by contacting the Cambridge Crystallographic Data Centre, 12 Union Road, Cambridge CB2 1EZ, UK; fax: +44 1223 336033.

Acknowledgements

We gratefully acknowledge the ITMZ (at the University of Rostock) for providing access to the cluster computer, and we especially thank Malte Willert for his assistance with the queueing system and software installations. We further acknowledge financial support from the graduate school RTG 2943 (“SPECTRE”, project code 507189291; Z.T., O.S.B., and R.R.) and from the DFG (1170/14-1; K.P.L.), and from the Leibniz Association through the Leibniz Competition (O.S.B.). We thank Peter Fritz and Joshua Sorst for their help with synthesis.

References

(1) Hinz, A.; Bresien, J.; Breher, F.; Schulz, A. Heteroatom-Based Diradical(Oid)S. *Chem. Rev.* **2023**, *123* (16), 10468–10526. https://doi.org/10.1021/acs.chemrev.3c00255.

(2) Bresien, J.; Eickhoff, L.; Schulz, A.; Zander, E. Biradicals in Main Group Chemistry: Synthesis, Electronic Structure, and Application in Small-Molecule Activation. In *Comprehensive Inorganic Chemistry III*; Elsevier, 2023; pp 165–233. https://doi.org/10.1016/B978-0-12-823144-9.00029-7.

(3) Stuyver, T.; Chen, B.; Zeng, T.; Geerlings, P.; De Proft, F.; Hoffmann, R. Do Diradicals Behave Like Radicals? *Chem. Rev.* **2019**, *119* (21), 11291–11351. https://doi.org/10.1021/acs.chemrev.9b00260.

(4) Zeng, Z.; Shi, X.; Chi, C.; López Navarrete, J. T.; Casado, J.; Wu, J. Pro-Aromatic and Anti-Aromatic π-Conjugated Molecules: An Irresistible Wish to Be Diradicals. *Chem. Soc. Rev.* **2015**, *44* (18), 6578–6596. https://doi.org/10.1039/C5CS00051C.

(5) González-Gallardo, S.; Breher, F. Main Group Biradicaloids. *Comprehensive Inorganic Chemistry II*. Elsevier 2013, pp 413–455. https://doi.org/10.1016/B978-0-08-097774-4.00118-2.

(6) Abe, M.; Borden, W. T.; Abe, M. Diradicals. *Chem. Rev.* **2013**, *113* (9), 7011–7088. https://doi.org/10.1021/cr400056a.

(7) Breher, F. Stretching Bonds in Main Group Element Compounds—Borderlines between Biradicals and Closed-Shell Species. *Coord. Chem. Rev.* **2007**, *251* (7–8), 1007–1043. https://doi.org/10.1016/j.ccr.2006.09.007.

(8) Salem, L.; Rowland, C. The Electronic Properties of Diradicals. *Angew. Chem. Int. Ed.* **1972**, *11* (2), 92–111. https://doi.org/10.1002/anie.197200921.

(9) Morozova, I. D.; Dyatkina, M. E. New Data on Biradicals. *Russ. Chem. Rev.* **1968**, *37* (5), 376–391. https://doi.org/10.1070/rc1968v037n05abeh001649.

(10) Hinz, A.; Schulz, A.; Villinger, A. Tunable Cyclopentane-1,3-Diyls Generated by Insertion of Isonitriles into Diphosphadiazanediyls. *J. Am. Chem. Soc.* **2015**, *137* (31), 9953–9962. https://doi.org/10.1021/jacs.5b05596.

(11) Fritz, P.; AlHamwi, H.; Villinger, A.; Michalik, D.; Bresien, J.; Reiß, F.; Beweries, T.; Schulz, A. A Phosphorus-Centred, Zirconocene-Bridged Tetraradical: Synthesis, Structure and Application as Molecular Double Switch. *Chem. – A Eur. J.* **2024**, *30*, e202402415. https://doi.org/10.1002/chem.202402415.

(12) Zander, E.; Bresien, J.; Zhivonitko, V. V.; Fessler, J.; Villinger, A.; Michalik, D.; Schulz, A. Rational Design of Persistent Phosphorus-Centered Singlet Tetraradicals and Their Use in Small-Molecule

Activation. *J. Am. Chem. Soc.* **2023**, *145* (26), 14484–14497. https://doi.org/10.1021/jacs.3c03928.

(13) Scheschkewitz, D.; Amii, H.; Gornitzka, H.; Schoeller, W. W.; Bourissou, D.; Bertrand, G. Singlet Diradicals: From Transition States to Crystalline Compounds. *Science* **2002**, *295* (5561), 1880–1881. https://doi.org/10.1126/science.1068167.

(14) Rodriguez, A.; Tham, F. S.; Schoeller, W. W. W.; Bertrand, G. Catenation of Two Singlet Diradicals: Synthesis of a Stable Tetraradical (Tetraradicaloid). *Angew. Chem. Int. Ed.* **2004**, *43* (37), 4876–4880. https://doi.org/10.1002/anie.200460473.

(15) Jin, X. Y.; Wang, J. Y.; Yang, X.; Chen, Z. N. Attaining Exceptional Stable Copper(I) Metallacyclopentadiene Diradicaloids through Ligand Engineering. *Inorg. Chem.* **2023**, *62* (47), 19323–19331. https://doi.org/10.1021/acs.inorgchem.3c03067.

(16) Godemann, C.; Hollmann, D.; Kessler, M.; Jiao, H.; Spannenberg, A.; Brückner, A.; Beweries, T. A Model of a Closed Cycle of Water Splitting Using Ansa -Titanocene(III/IV) Triflate Complexes. *J. Am. Chem. Soc.* **2015**, *137* (51), 16187–16195. https://doi.org/10.1021/jacs.5b11365.

(17) Godemann, C.; Dura, L.; Hollmann, D.; Grabow, K.; Bentrup, U.; Jiao, H.; Schulz, A.; Brückner, A.; Beweries, T. Highly Selective Visible Light-Induced Ti–O Bond Splitting in an Ansa-Titanocene Dihydroxido Complex. *Chem. Commun.* **2015**, *51* (15), 3065–3068. https://doi.org/10.1039/C4CC09733E.

(18) Kessler, M.; Schüler, S.; Hollmann, D.; Klahn, M.; Beweries, T.; Spannenberg, A.; Brückner, A.; Rosenthal, U. Photoassisted Ti□O Activation in a Decamethyltitanocene Dihydroxido Complex: Insights into the Elemental Steps of Water Splitting. *Angew. Chem. Int. Ed.* **2012**, *51* (25), 6272–6275. https://doi.org/10.1002/anie.201202097.

(19) No Title. https://doi.org/10.1002/chem.70968.

(20) Pilopp, Y.; Bresien, J.; Gschwind, D. T.; Villinger, A.; Michalik, D.; Schulz, A. Access to Benzo- and Naphtho-Azaphospholes via C−H Bond Activation of Aryl-Substituted Isonitriles. *Chem. – A Eur. J.* **2023**, *29* (33), e202300764. https://doi.org/10.1002/chem.202300764.

(21) Bresien, J.; Kröger-Badge, T.; Lochbrunner, S.; Michalik, D.; Müller, H.; Schulz, A.; Zander, E. A Chemical Reaction Controlled by Light-Activated Molecular Switches Based on Hetero-Cyclopentanediyls. *Chem. Sci.* **2019**, *10*, 3486–3493. https://doi.org/10.1039/C8SC04893B.

(22) Weigend, F.; Ahlrichs, R. Balanced Basis Sets of Split Valence, Triple Zeta Valence and Quadruple Zeta Valence Quality for H to Rn: Design and Assessment of Accuracy. *Phys. Chem. Chem. Phys.* **2005**, *7* (18), 3297. https://doi.org/10.1039/b508541a.

(23) Hellweg, A.; Hättig, C.; Höfener, S.; Klopper, W. Optimized Accurate Auxiliary Basis Sets for RI-MP2 and RI-CC2 Calculations for the Atoms Rb to Rn. *Theor. Chem. Acc.* **2007**, *117* (4), 587–597. https://doi.org/10.1007/s00214-007-0250-5.

(24) Riplinger, C.; Neese, F. An Efficient and near Linear Scaling Pair Natural Orbital Based Local Coupled Cluster Method. *J. Chem. Phys.* **2013**, *138* (3), 034106. https://doi.org/10.1063/1.4773581.

(25) Liakos, D. G.; Guo, Y.; Neese, F. Comprehensive Benchmark Results for the Domain Based Local Pair Natural Orbital Coupled Cluster Method (DLPNO-CCSD(T)) for Closed- and Open-Shell Systems. *J. Phys. Chem. A* **2020**, *124* (1), 90–100. https://doi.org/10.1021/acs.jpca.9b05734.

(26) Liakos, D. G.; Sparta, M.; Kesharwani, M. K.; Martin, J. M. L.; Neese, F. Exploring the Accuracy Limits of Local Pair Natural Orbital Coupled-Cluster Theory. *J. Chem. Theory Comput.* **2015**, *11* (4), 1525–1539. https://doi.org/10.1021/ct501129s.

(27) Riplinger, C.; Pinski, P.; Becker, U.; Valeev, E. F.; Neese, F. Sparse Maps—A Systematic Infrastructure for Reduced-Scaling Electronic Structure Methods. II. Linear Scaling Domain Based Pair Natural Orbital Coupled Cluster Theory. *J. Chem. Phys.* **2016**, *144* (2), 024109. https://doi.org/10.1063/1.4939030.

(28) Pracht, P.; Bohle, F.; Grimme, S. Automated Exploration of the Low-Energy Chemical Space with Fast Quantum Chemical Methods. *Phys. Chem. Chem. Phys.* **2020**, *22* (14), 7169–7192. https://doi.org/10.1039/c9cp06869d.

(29) Grimme, S.; Bohle, F.; Hansen, A.; Pracht, P.; Spicher, S.; Stahn, M. Efficient Quantum Chemical Calculation of Structure Ensembles and Free Energies for Nonrigid Molecules. *J. Phys. Chem. A* **2021**, *125* (19), 4039–4054. https://doi.org/10.1021/acs.jpca.1c00971.

(30) Pyykkö, P.; Atsumi, M. Molecular Double-Bond Covalent Radii for Elements Li-E112. *Chem. Eur. J.* **2009**, *15* (46), 12770–12779. https://doi.org/10.1002/chem.200901472.

(31) Alvarez, S. A Cartography of the van Der Waals Territories. *Dalton Trans.* **2013**, *42* (24), 8617–8636. https://doi.org/10.1039/c3dt50599e.

(32) Miliordos, E.; Ruedenberg, K.; Xantheas, S. S. Unusual Inorganic Biradicals: A Theoretical Analysis. *Angew. Chem.* **2013**, *125* (22), 5848–5851. https://doi.org/10.1002/ange.201300654.

(33) Beweries, T.; Kuzora, R.; Rosenthal, U.; Schulz, A.; Villinger, A. [P(μ-NTer)]2: A Biradicaloid That Is Stable at High Temperature. *Angew. Chem. Int. Ed.* **2011**, *50* (38), 8974–8978. https://doi.org/10.1002/anie.201103742.

(34) Hinz, A.; Kuzora, R.; Rosenthal, U.; Schulz, A.; Villinger, A. Activation of Small Molecules by Phosphorus Biradicaloids. *Chem. Eur. J.* **2014**, *20* (45), 14659–14673. https://doi.org/10.1002/chem.201403964.

(35) Bresien, J.; Schulz, A.; Szych, L. S.; Villinger, A.; Wustrack, R. [E(μ-NBbp)] 2 (E = P, As) – Group 15 Biradicals Synthesized from Acyclic Precursors. *Dalton Trans.* **2019**, *48* (29), 11103–11111. https://doi.org/10.1039/C9DT01654F.

(36) Hinz, A.; Schulz, A.; Villinger, A. Metal-Free Activation of Hydrogen, Carbon Dioxide, and Ammonia by the Open-Shell Singlet Biradicaloid [P(μ-NTer)] 2. *Angew. Chem. Int. Ed.* **2016**, *55* (40), 12214–12218. https://doi.org/10.1002/anie.201606892.

(37) Herzberg, G. *Molecular Spectra and Molecular Structure. Vol. I: Spectra of Diatomic Molecules*; Van Nostrand Reinhold: New York, 1950.

Supplementary Files

This is a list of supplementary files associated with this preprint. Click to download.

- esisubmitted.pdf